Journal of Catalysis 274 (2010) 192–199

Contents lists available at ScienceDirect

Journal of Catalysis

journal homepage: www.elsevier.com/locate/jcat

Synthesis and characterization of a new catalyst Pt/Mg(Ga)(Al)O for alkane dehydrogenation

Pingping Sun [a], Georges Siddiqi [a], Miaofang Chi [b], Alexis T. Bell [a,*]

[a] Department of Chemical Engineering, University of California, Berkeley, CA 94720-1462, United States
[b] Oak Ridge National Laboratory, Oak Ridge, TN 37831-6064, United States

ARTICLE INFO

Article history:
Received 7 May 2010
Revised 28 June 2010
Accepted 29 June 2010
Available online 10 August 2010

Keywords:
Pt bimetallic catalyst
Mg(Ga)(Al)O support
STEM
EXAFS
Dehydrogenation

ABSTRACT

A novel approach is described for preparing Ga-promoted Pt particles for the dehydrogenation of light alkanes to alkenes. The modifying element, Ga, was introduced by transference from the support, a calcined Mg(Ga)(Al)O hydrotalcite-like material. Pt nanoparticles were dispersed onto the calcined Mg(Ga)(Al)O starting from an organometallic precursor, followed by reduction. The formation of PtGa alloy particles is dependent on reduction temperature. Reduction at 723 K produces mainly metallic Pt particles. The average diameter of the Pt nanoparticles increased from 1.4 nm to 2.2 nm with increasing Ga content, and decreasing Al content of the support, demonstrating the importance of support Al atoms in stabilizing the dispersion of Pt. After reduction at 773–873 K, PtGa alloys were observed. It is proposed that at high reduction temperatures, H atoms formed on the surface of the metal particles spill over onto the support where they reduce Ga^{3+} cation to atomic Ga, which then interacts with the supported Pt to form PtGa alloys. The activity, selectivity and stability of Pt/Mg(Ga)(Al)O catalysts for ethane and propane dehydrogenation are described in the second part of this study (G. Siddiqi, P. Sun, V. Galvita, A.T. Bell, Journal of catalysis (2010), doi:10.1016/j.jcat.2010.06.016 [40]).

1. Introduction

Light alkenes, such as ethylene, propylene, and *n*-butene, are widely used as building blocks for the production of commodity chemical and polymers. Rising demand for light alkenes has exceeded the capacity for the production of these products by petroleum cracking, the current principal source, motivating an interest for seeking other means for producing intermediates. The catalytic dehydrogenation of ethane, propane, and butane offers an attractive alternative source, since the starting materials are inexpensive. A further attraction of alkane dehydrogenation is that hydrogen, the principal byproduct, is a valuable commodity that can readily be used for many purposes within a petroleum refinery, e.g., hydrocracking and heteroatom removal.

Platinum is known as an active catalyst for the dehydrogenation of light alkanes, but in the absence of modifiers suffers from low alkene selectivity and deactivation due to rapid coke formation. Alkene selectivity can be increased, and the tendency to form coke decreased by promoting Pt with elements, such as Sn, Zn, Ge, Pb, and Re [1–6]. The means by which the promoting element interacts with Pt and influences its catalytic properties are best understood for Sn. EXAFS [7–9], Mossbauer [10–12], and TEM [13–15] studies of supported SnPt catalysts suggest that Sn forms a variety of bimetallic alloys, which enhance the dissociative adsorption of the reacting alkane and attenuate the adsorption of the product alkene [16–28]. The first of these effects increases the rate of alkene formation, whereas the latter reduces the loss of hydrogen from the readsorbed alkene, a process that leads to the formation of lower molecular weight products and coke [29,30]. The composition of the support used for Pt bimetallic catalysts influences the stability of the metal particles to sintering and the formation of coke on the support itself. Previous studies have shown that the formation of coke is minimized using non-acidic supports such as K–L zeolite, alkali-doped alumina, spinels, and calcined hydrotalcite [Mg(Al)O] [31–36]. Of these supports, Mg(Al)O is particularly attractive because it is moderately basic and exhibits high thermal stability to steam and reaction–oxidation cycling [37,38].

In a recent study [39], we have shown that PtSn/Mg(Al)O is a highly active and selective catalyst for the dehydrogenation of ethane to ethene. The support was produced by calcining a hydrotaclite-like precursor prepared with an Mg/Al ratio of 5. The BET area of the calcined support was 200 m^2/g. Pt nanoparticles were deposited by impregnation of the support with a toluene solution of $Pt(acetylacetonate)_2$, drying, and H_2 reduction. To achieve intimate contact between the Sn precursor and the Pt particles, reduced Pt/Mg(Al)O was reacted with tetrabutyl tin and then reduced in H_2. The highest dehydrogenation activity was obtained with a Sn/Pt ratio of 0.3, whereas 100% ethene selectivity was achieved for a Sn/Pt ratio of 0.4, with only a small loss in dehydrogenation activity.

* Corresponding author. Fax: +1 510 642 4778.
E-mail address: bell@cchem.berkeley.edu (A.T. Bell).

0021-9517/$ - see front matter © 2010 Elsevier Inc. All rights reserved.
doi:10.1016/j.jcat.2010.06.017

A further attraction of hydrotalcite-derived supports is that they can be prepared with elements other than Al, e.g., Zn, Ga, In. We have recently exploited this characteristic by preparing and evaluating a series of Pt/Mg(Ga)(Al)O catalysts for the dehydrogenation of ethane and propane. This paper focuses on the synthesis and characterization of these catalysts, whereas the second one focuses on the evaluation of these catalysts for ethane and propane dehydrogenation [40].

2. Experimental

2.1. Catalyst synthesis

Mg(Ga)(Al)O was synthesized using the following procedure: 58.31 g of $Mg(NO_3)_2{\cdot}6H_2O$ (Alfa Aesar, 98–102%), an appropriate amount (depending on the desired Ga/Al ratio) of $Al(NO_3)_3{\cdot}9H_2O$ (Alfa Aesar, 98–102%) and an appropriate amount of $Ga(NO_3)_3{\cdot}xH_2O$ (Alfa Aesar, 99.9%) were dissolved in 250 ml of deionized water, and 1.2 g of Na_2CO_3 (EMD Chemicals Inc., 99.5%) and 11 g of NaOH (Fisher Scientific, 98.3%) were dissolved in 250 ml of deionized water. These two solutions were mixed by dropwise addition over a period of about 20 min in a stirred vessel maintained at about 333 K, afterward the mixture was taken out of water bath then aged at RT for 18 h. The aged solution was then filtered, and the solid product dried overnight in air at 383 K. The dried material was heated in air to 973 K at 2 K/min and maintained at this temperature for 10 h to obtain the final support, which we describe as Mg(Ga)(Al)O. Pure Mg(Ga)O and Mg(Al)O were prepared in a similar manner.

Pt was dispersed onto the calcined support via grafting. Twenty-one milligrams of $Pt(acetylacetonate)_2$ (Sigma Aldrich, 99.99%) was dissolved in 1.5 ml toluene. This solution was then poured onto 1 g of freshly calcined support. The resulting slurry mixture was stirred until it became powdery, then left at room temperature in air for 2 h, and finally dried overnight at 383 K in an oven. After drying, the catalyst was reduced at 723 K for 2 h (5 K/min temperature ramp) in 10% H_2/Ar (60 cm^3/min), referred to as the as-prepared catalyst.

2.2. Catalyst characterization

The Pt, Mg, Al, Ga contents of all samples were determined by Galbraith Laboratories (Knoxville, TN) by inductively coupled plasma optical emission spectroscopy. The surface area of Pt/Mg(Ga)(Al)O was determined by the multi-point method using an Autosorb-1 instrument (Quantachrome Corporation, Boynton Beach, FL). Prior to measuring the adsorption isotherm, each sample was degassed under vacuum at 573 K for 22–24 h. The structure of the support material was characterized by X-ray powder diffraction before and after calcination, using a Siemens Diffractometer D 5000 with CuKα radiation (λ = 1.5418 Å) at 20 kV and 5 mA. The samples were scanned from 2θ values of 5° to 70° with a step size of 0.02° and a dwell time of 1.0 s.

Thermogravimetric analysis (TGA) and differential scanning calorimeter (DSC) were used to characterize the transformations occurring during calcination of the dried support. These measurements were performed with a TA Instrument, SDT 2960 Simultaneous DSC-TGA. About 20 mg of the dried, as-synthesized support was placed in an alumina crucible and heated from 403 to 1173 K in flowing nitrogen (100 cm^3/min) at a rate of 10 K/min.

Magic angle spinning (MAS) ^{71}Ga NMR spectra were acquired on a Bruker Avance 500 MHz NMR spectrometer equipped with a broadband, double resonance, magic angle spinning (MAS) probe tuned to 152.55 MHz. Samples were spun at frequencies between 7 and 12 kHz in zirconia rotors of 4 mm outer diameter and 80 μL sample volume. ^{71}Ga spectra were obtained using a solid echo sequence ($(\pi/2) - \tau - (\pi/2)$) with a 90° pulse of 4.5 μs and τ value of ~18 μs. A recycle delay of 0.1 s and scans up to 400,000 were used. The spectra were referenced using 1 M $Ga(NO_3)_3$ at 0 ppm.

The dispersion of Pt was determined by H_2 chemisorption using a AutoChem II 2920 (Micromeritics Instrument Corporation). About 60 mg of Pt/Mg(Ga)(Al)O was loaded into a quartz cell and then reduced in flowing 10% H_2/Ar (50 cm^3/min). The temperature of the sample was raised at 5 K/min to 873 K and then maintained at this level for 2 h. The sample was then flushed in flowing Ar for 90 min and then cooled down to 318 K. The uptake of chemisorbed hydrogen was then measured by determining the uptake of H_2 from pulses using a TCD detector. The pulse size was 50 cm^3/g and the time between pulses was 10 min.

Pt L_{III} edge EXAFS data were obtained at the Stanford Synchrotron Radiation Laboratory (SSRL) using Beamline 4-1. As-prepared catalyst samples (reduced at 723 K after $Pt(acac)_2$ deposition) were pressed into wafers and then placed into a stainless steel cell in which the sample could be heated or cooled in the presence of flowing gas. EXAFS data of as-prepared catalysts were acquired with He flowing through the cell at 60 cm^3/min. To acquire the active metallic particle information under reaction state, the sample was reduced in 10% H_2/Ar (500 °C for Pt/Mg(Ga)(Al)O Ga/Pt = 5.4 and 873 K for Pt/Mg(Ga)(Al)O Ga/Pt = 12) for 2 h with flowing rate of 60 cm^3/min and heating rate of 10 K/min. The sample was then cooled to liquid nitrogen temperature and maintained at that temperature for all measurements. Background removal, normalization and other data processing were done using "Athena", and the fitting of theoretical standards to the experimental data was done using "Artemis" [41,42]. Theoretical standards were constructed using known crystal structures of PtGa alloys, as well as Pt oxides [43,44].

The structure of the support was examined using a FEI Tecnai 12 transmission electron microscope. Samples were prepared by placing a small amount (<10 mg) of sample in ethanol and sonicating for 15 min. The mixture was then added via a dropper onto a holey carbon-coated grid deposited on a 200-mesh copper screen (S.P.I. Supplies) and allowed to dry in air.

STEM-EDX analyses were conducted by Evans Analytical Group (Sunnyvale, CA) using a FEI Tecnai TF-20XT FEGTEM equipped with a 30 mm 2 INCA EDS detector. The STEM operated at 200 kV acceleration potential. High Angle Annular Dark Field-Scanning Transmission Electron Microscopy (HAADF-STEM) images were acquired from the catalyst nanoparticles. The nominal electron probe size was about 1.5 nm in diameter. The samples had been supported on a lacey carbon support film on copper mesh grid. Point and areal EDS spectra were obtained for the energy range of 0–20 keV.

3. Results and discussion

A list of all samples studied is presented in Table 1. The Mg/(Al + Ga) ratio was maintained close to 5 for the majority of the samples, as the Al/Ga ratio was varied from 0 to ∞. The Pt content was maintained between 0.7 wt% and 0.8 wt%, which means that the bulk Ga/Pt ratio was varied from 0 to 96.

Fig. 1 shows the XRD pattern of the dried, as-synthesized support (bottom) and the same material after calcination (top). Prior to calcination, the XRD pattern is characteristic of the layered double hydroxide structure of hydrotalcite [45]. After calcination at 973 K, the structure of the solid changes from orthorhombic to a cubic, corresponding to the transformation of a two-dimensional layered structure to a three-dimensional structure, analogous to periclase MgO. The broad peaks of both materials are indicative

Table 1
Material properties of synthesized Pt/Mg(Ga)(Al)O catalysts.

Sample name	Pt wt%	Ga wt%	Starting ratio Mg:Al:Ga	Mg(Al + Ga)	Al/Ga	Ga/Pt
Pt/Mg(Al)O	0.696	0	100:10:0	5.09	–	–
Pt/Mg(Al)(Ga)O-0.30	0.801	0.082	100:9.95:0.05	5.59	267	0.3
Pt/Mg(Al)(Ga)O-1.4	0.796	0.403	100:9.75:0.25	5.21	56	1.4
Pt/Mg(Al)(Ga)O-2.0	0.807	0.573	100:29:1	4.97	39.8	2.0
Pt/Mg(Al)(Ga)O-2.9	0.679	0.694	100:19:1	5.18	28.8	2.9
Pt/Mg(Al)(Ga)O-5.4	0.884	1.72	100:9:1	5.15	13	5.4
Pt/Mg(Al)(Ga)O-12	0.765	3.22	100:8:2	5.46	5.9	12
Pt/Mg(Al)(Ga)O-30	0.717	6.24	100:5:5	3.81	2.9	30
Pt/Mg(Ga)O-61	0.835	18.3	100:0:20	6.24	0	61.3
Pt/Mg(Ga)O-96	0.825	28.3	100:0:33	3.12	0	96

The letter refers to support name, the digit afterward refer to Ga/Pt ratio of the catalyst.

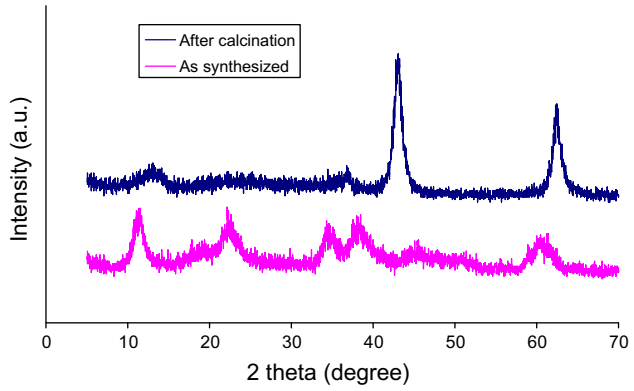

Fig. 1. XRD pattern of as-synthesized and calcined HTMg(Al)(Ga)O of 3.22 wt% Ga.

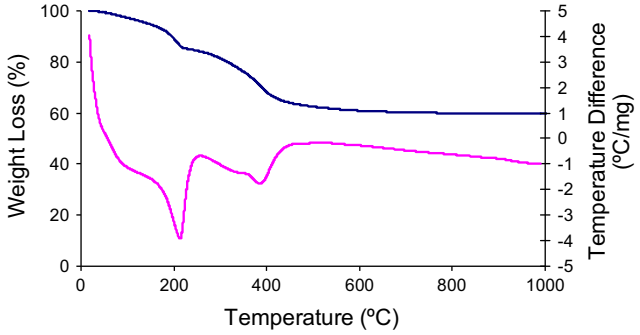

Fig. 3. TGA-DSC diagram of hydrotalcites HTMgGaO with 28.3 wt% Ga.

of small crystalline particles or a partially amorphous phase. Similar changes in the XRD patterns were observed for all support materials, independent of the Al/Ga ratio.

Fig. 2 shows the thermogravimetric analysis-differential scanning calorimetry (TGA-DSC) curve of the dried, as-prepared support containing 3.22 wt% Ga (Al/Ga = 6), whereas Fig. 3 shows the TGA-DSC curve of the dried support containing 28.3 wt% Ga (Al/Ga = 0). The two materials exhibit similar TGA-DSC patterns. Two endothermic peaks are observed, one below 573 K, corresponding to the release of interlayer water, and the other between 573 K and 873 K, corresponding to dehydroxylation and carbonate decomposition [46–48]. With increasing Ga content, the first peak shifts to higher temperatures, while the second peak shifts to lower temperatures. A small endothermic peak starting at 1173 K was also observed, which may correspond to the formation of a dense spinel phase [49]. A loss in sample weight was observed up to 973 K, and as a result, this temperature was chosen as the upper limit needed to obtain a dry, high surface area support without inducing the transition to a dense spinel phase.

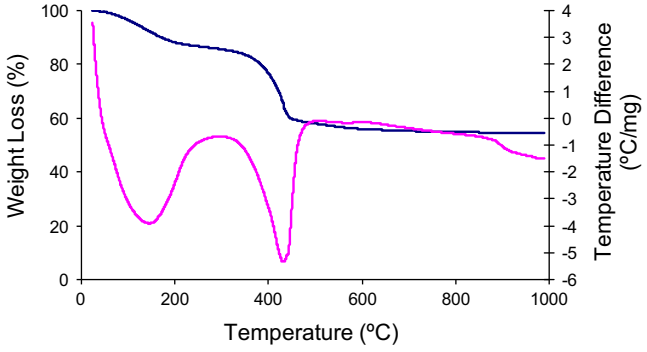

Fig. 2. TGA-DSC diagram of HTMgAlGaO with 3.22 wt% Ga.

The TGA measurements revealed that the endothermic peaks shifted with increasing Ga content. The first peak shifted to a higher temperature, indicating that the Ga-containing material holds water more tightly, and the second peak shifted to lower temperatures, indicating that the presence of Ga facilitates the decomposition of the hydrotalcite to mixed oxides. The latter change is very likely due to the more random layer stacking of Mg–Ga type hydrotalcites compared to Mg–Al type hydrotalcites [45].

Table 2 lists the surface areas of the calcined mixed oxide materials. Mg(Al)O has a surface area of 176 m^2/g and a pore volume of 0.6 cm^3/g. The addition of Ga to the hydrotalcite-like precursor material caused a small decrease in the surface area of the calcined support as well as the pore volume. While not shown, the surface area and pore volume changed minimally upon the dispersion of Pt onto the support.

The local order of Ga atoms in Pt/Mg(Ga)(Al)O was probed by ^{71}Ga NMR. Fig. 4 shows the ^{71}Ga NMR spectra of three samples containing Pt loading of about 0.8 wt%, but with different Ga/Pt ratios. Spectrum A (Ga/Pt = 5.4) exhibits peaks at 32.1 and 12.1 ppm, characteristic of Ga in octahedral coordination. The presence of two peaks is due to two types of octahedrally coordinated Ga, differing in the presence of Mg or Mg and Al in the second nearest-neighbor coordination sphere [50]. As seen in spectrum B, increasing the Ga/Pt ratio to 12 had no detectable effect on the ^{71}Ga NMR spectrum. However, further increasing the Ga/Pt ratio to 96 (spectrum C) resulted in the occurrence of additional peaks at 58.2 ppm and 201.1 ppm, characteristic of Ga cations with five- and fourfold coordination [51–53], suggesting that at high Ga/Pt ratios, the coordination of Ga changes. EXAFS studies probe into the local ordering Ga atoms in calcined hydrotalcites Mg(Ga)O by Bellotto et al. [45] have shown that for Mg/Ga ratios greater than 3, the four-coordinated Ga atoms may be due to formation of spinel structure, whereas five-coordinated Ga may be due to unsaturated

Table 2
Chemisorption and physisorption results of Pt/Mg(Ga)(Al)O catalysts over a range of Ga/Pt ratios.

Sample name	Dispersion (%)	Average particle size (nm)	Surface area (m^2/g)	Pore volume (cc/g)	Average radius (Å)
Pt/Mg(Al)O	84	1.35	176	0.60	70.0
Pt/Mg(Al)(Ga)O-0.29	67.8	1.67	173	0.52	59.8
Pt/Mg(Al)(Ga)O-1.4	78	1.45	160	0.66	82.6
Pt/Mg(Al)(Ga)O-2.0	76.0	1.51	162	0.46	57.0
Pt/Mg(Al)(Ga)O-2.9	71.2	1.59	161	0.41	51.3
Pt/Mg(Al)(Ga)O-5.4	70.5	1.6	148	0.52	70.2
Pt/Mg(Al)(Ga)O-12	78.7	1.44	142	0.49	68.4
Pt/Mg(Al)(Ga)O-30	72.6	1.6	129	0.44	67.8
Pt/Mg(Ga)O-61	56.5	2.0	107	0.43	80.3
Pt/Mg(Ga)O-96	52.3	2.2	138	0.65	94.2

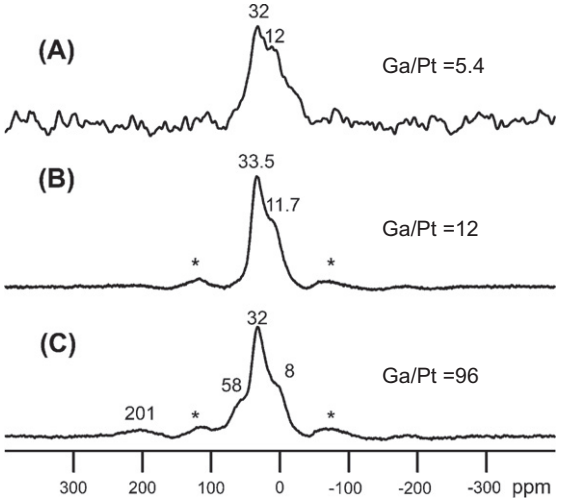

Fig. 4. (A) Pt/Mg(Al)(Ga)O-5.4, ν = 12 kHz with 1700 scans. (B) Pt/Mg(Al)(Ga)O-12, ν = 12 kHz, with 505,000 scans. (C) Pt/Mg(Ga)O-96 shows peaks at 58 ppm and 201 ppm ν = 12 kHz, 21,000 scans (peak at 58 ppm confirmed by spinning at 7 kHz).

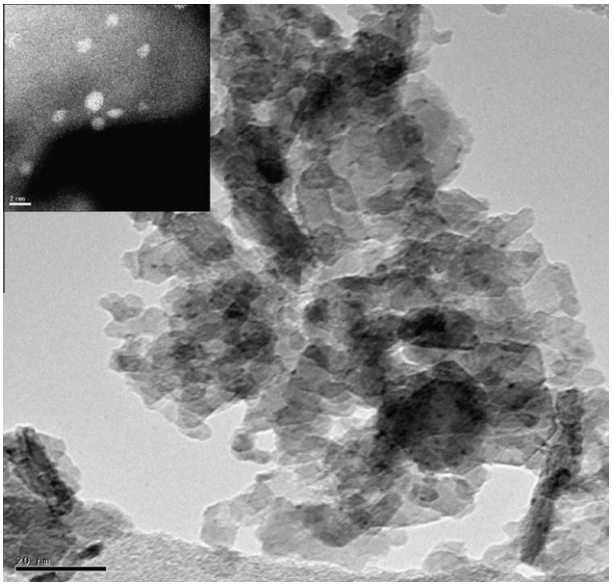

Fig. 5. TEM micrograph of Pt/Mg(Ga)(Al)O with Ga/Pt = 5.4, inset shows HAADF-STEM micrograph of same catalyst, bright areas represent metals.

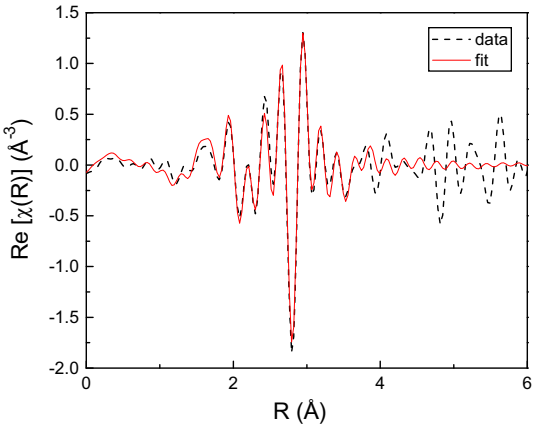

Fig. 6. k^2-weighted EXAFS of Pt/Mg(Ga)(Al)O with Ga/Pt = 5.4, reduced at 723 K. Data are shown in dashed line, fit of theoretical structure in solid line.

surface formed species by dehydroxylation upon calcinations. Thus, the appearance of four- and fivefold coordinated Ga in Pt/Mg(Ga)(Al)O-96 is attributed to restructuring of the support.

The dispersion of the Pt particles on calcined hydrotalcite-like supports, determined by H_2 chemisorption, is presented in Table 2. Pt supported on Mg(Al)O has a dispersion of 84%, corresponding to an average particle size of 1.35 nm. The dispersion of Pt on Mg(Ga)(Al)O tended to decrease with increasing Ga/Pt ratio from about 78% to 52%, corresponding to an increase in average Pt particle size from 1.5 to 2.2 nm. The observed decrease in Pt dispersion with increasing Ga/Pt ratio is very likely due to the decrease in the concentration of Al cations at the surface of the support, which have been observed to facilitate the dispersion of Pt [54].

A TEM image of Pt/Mg(Ga)(Al)O-5.4 is shown in Fig. 5. After calcination, the support still exhibited a layered structure, similar to that seen earlier for Mg(Al)O [55]. Small Pt particles about 1–2 nm in diameter are also seen. Lattice images of these small particles can be seen in the high-resolution micrograph shown as an inset in Fig. 5. The sizes of these particles are consistent with the average particle size deduced from H_2 chemisorption.

Evidence for the interactions of Ga with Pt was obtained from EXAFS. Pt L_{III} edge EXAFS data were acquired for as-prepared Pt/Mg(Ga)(Al)O Ga/Pt = 5.4 and Pt/Mg(Ga)(Al)O Ga/Pt = 12, reduced in H_2 at 723 K, and following reduction of 773 K (Pt/Mg(Ga)(Al)O Ga/Pt = 5.4) and 873 K (Pt/Mg(Ga)(Al)O Ga/Pt = 12). The results are shown in Figs. 6 and 7. Analysis of the EXAFS pattern of as-prepared Pt/Mg(Ga)(Al)O Ga/Pt = 5.4 gives Pt–Pt (d_{Pt-Pt} = 2.77 Å) and Pt–O (d_{Pt-O} = 2.05 Å) coordination numbers of 4.4 ± 0.6 and 1.1 ± 0.2, respectively. A similar analyses for Pt/Mg(Ga)(Al)O Ga/Pt = 12 gives a Pt–Pt (d_{Pt-Pt} = 2.77 Å) and Pt–O (d_{Pt-O} = 2.03 Å) coordination numbers of 3.9 ± 0.6 and 1.2 ± 0.2, respectively. Thus, EXAFS analysis suggests that after reduction at 723 K, platinum is present as a mixture of Pt and PtO_x.

The EXAFS pattern acquired after the reduction of Pt/Mg(Ga)(Al)O-5.4 at 873 K is shown in Fig. 8. A good fit of the pattern could be obtained using EXAFS parameters for pure Pt and PtGa. By this

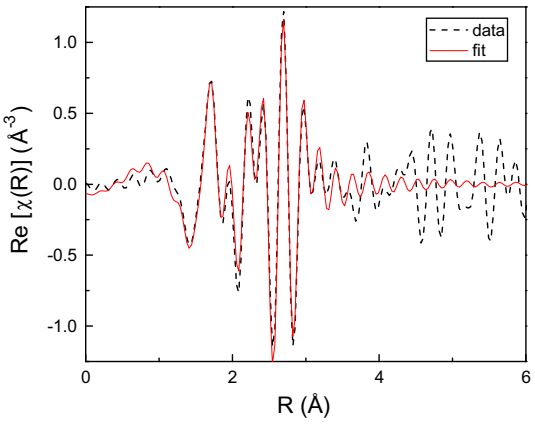

Fig. 7. k^2-weighted EXAFS of Pt/Mg(Ga)(Al)O of Ga/Pt = 12, reduced at 723 K. Data are shown in dashed line, fit of theoretical structure in solid line.

means, the Pt–Pt coordination (d_{Pt-Pt} = 2.79 Å) was found to be 7.0 ± 0.5 and the Pt–Ga coordination (d_{Pt-Ga} = 2.53 Å) was found to be 1.2 ± 0.6, giving a total Pt coordination number of 8.14 ± 0.85. An even larger change in the EXAFS pattern was observed when as-prepared Pt/Mg(Ga)(Al)O-12 was reduced in H_2 at 873 K, in Fig. 9. In this case, the Pt–Pt coordination (d_{Pt-Pt} = 2.75 Å) was found to be 5.2 ± 1.0 and the Pt–Ga coordination (d_{Pt-Ga} = 2.58 Å) was found to be 3.6 ± 2.4, giving a total Pt coordination of 8.8 ± 3.3. The higher Pt–Ga coordination number for the sample with Ga/Pt = 12 indicates that an increase in the reduction temperature leads to a greater degree of association of Ga with Pt. It is also possible that the metal nanoparticles in Pt/Mg(Ga)(Al)O-12 are richer in Ga than those in sample with a Ga/Pt = 5.4 because of higher concentration of Ga in the bulk of the former catalyst. The close similarity in the total coordination number for Pt in both samples indicates that the particle sizes in the two samples are similar, in agreement with what was found by H_2 chemisorption.

The Ga K-edge XANES and EXAFS patterns taken of Pt/Mg(Ga)(Al)O-5.4 and Pt/Mg(Ga)(Al)O-12 reduced at 723 K and 873 K are shown in Fig. 10. Virtually, no change in the patterns is observed either with Ga/Pt ratio or temperature of reduction, indicating that most of the Ga remains in the support and that migration of only a small amount of Ga to the Pt is responsible for the significant change in Pt–Ga backscattering seen in Pt L_{III} edge EXAFS patterns.

Additional evidence for the formation of PtGa alloys was obtained from EDX analysis of the samples. EDX was conducted on

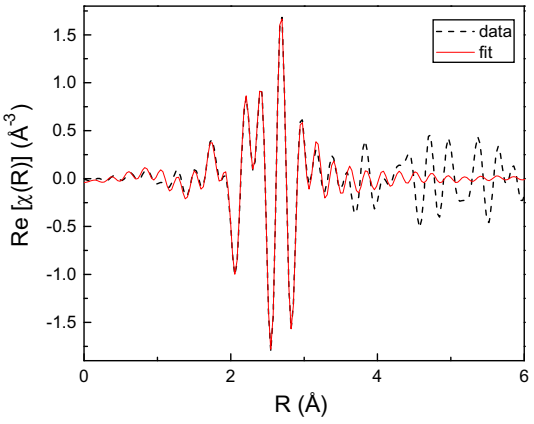

Fig. 8. k^2-weighted EXAFS of Pt/Mg(Ga)(Al)O with Ga/Pt = 5.4, reduced at 773 K. Data are shown in dashed line, fit of theoretical structure in solid line.

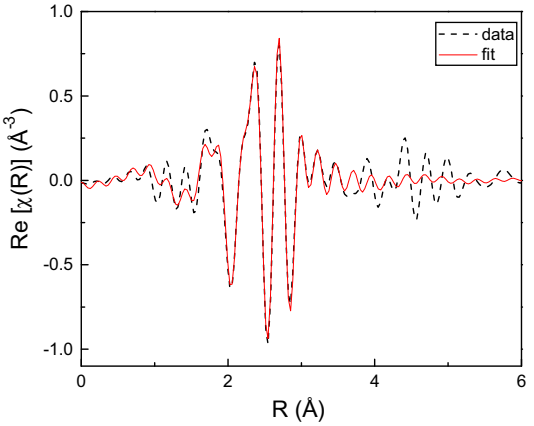

Fig. 9. k^2-weighted EXAFS of Pt/Mg(Ga)(Al)O of Ga/Pt = 12, reduced at 873 K. Data are shown in dashed line, fit of theoretical structure in solid line.

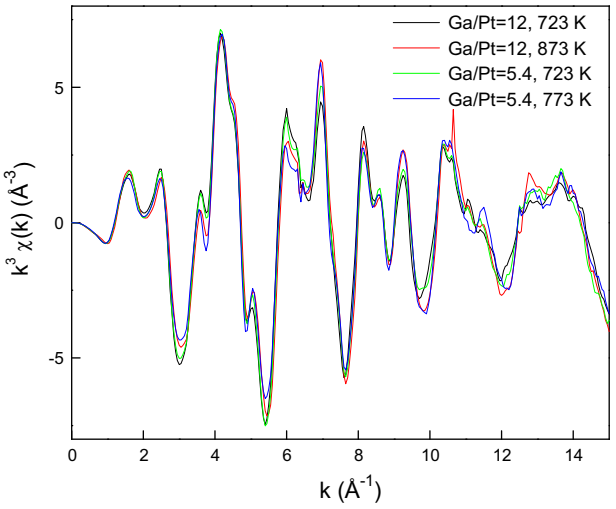

Fig. 10. Ga K-edge EXAFS of Pt/Mg(Ga)(Al)O of Ga/Pt = 5.4 and 12 at reduction temperatures ranging from 723 K to 873 K.

larger particles of Pt/Mg(Ga)(Al)O-5.4 and of Pt/Mg(Ga)(Al)O-12 after reduction at 723 K and 873 K. In areas of the support free of Pt particles, the Ga/Mg ratio measure after sample reduction at 723 K was for $1.37 \pm 0.23 \times 10^{-2}$ for Pt/Mg(Ga)(Al)O-5.4 and $2.28 \pm 0.5.1 \times 10^{-2}$ for Pt/Mg(Ga)(Al)O-12 in good agreement with the bulk stoichiometric values of 1.39×10^{-2} and 2.65×10^{-2}, respectively. Figs. 11 and 12 show the distribution of Ga/Pt ratios for of the metal particles characterized by EDX after reduction of Pt/Mg(Ga)(Al)O-5.4 and Pt/Mg(Ga)(Al)O-12 at 723 K. It is evident that for both samples, most of the Pt is unassociated with Ga, and only a small to modest fraction of the particles exhibit Ga/Pt ratios in the range of 0.01–0.10. A significant change was observed, though, after reduction at 873 K. In this case, Figs. 11 and 12 show that the Ga/Pt ratio of the Pt particles rises to between 0.1 and 0.59 for Pt/Mg(Ga)(Al)O-5.4 and between 0.1 and 1.09 for Pt/Mg(Ga)(Al)O-12. Thus, the average Ga/Pt ratio of the metal particles is larger, the larger the bulk value of Ga/Pt. It is significant that ICP analysis of Pt/Mg(Ga)(Al)O-10 (a duplicate of Pt/Mg(Ga)(Al)O-12) before and after reduction at 873 K gave Ga/Mg ratios of 2.78×10^{-2} and 2.69×10^{-2}. The difference in Ga/Mg rations is well within error range of ICP analysis, and, therefore, it is concluded that H_2 reduction at 873 K does not result in a loss of Ga from the catalyst. The non-uniformity of the Ga/Pt ratio seen in Figs. 11 and 12 after

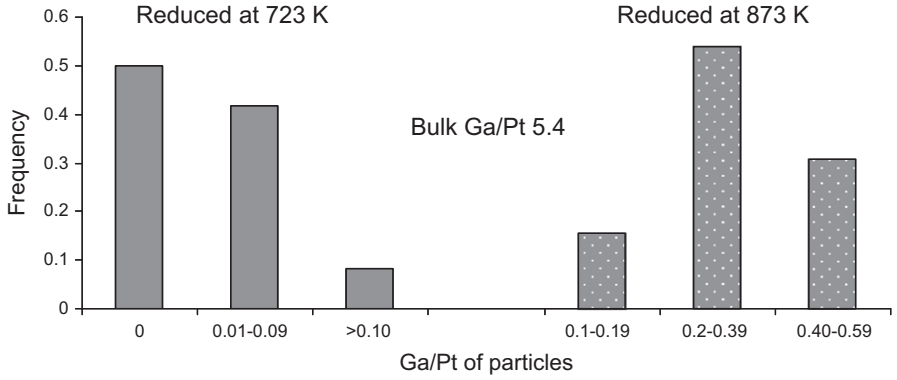

Fig. 11. The distribution of the Ga/Pt ratio present in Pt/Mg(Ga)(Al)O (Ga/Pt = 5.4) catalyst after reduction at either 723 K or 873 K. Obtained from STEM-EDX analysis of catalysts.

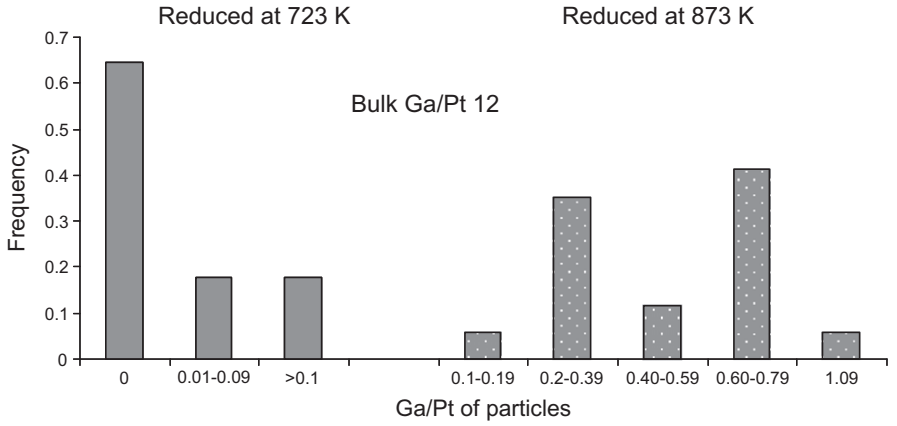

Fig. 12. The distribution of the Ga/Pt ratio present in Pt/Mg(Ga)(Al)O (Ga/Pt = 12) catalyst after reduction at either 723 K or 873 K. Obtained from STEM-EDX analysis of catalysts.

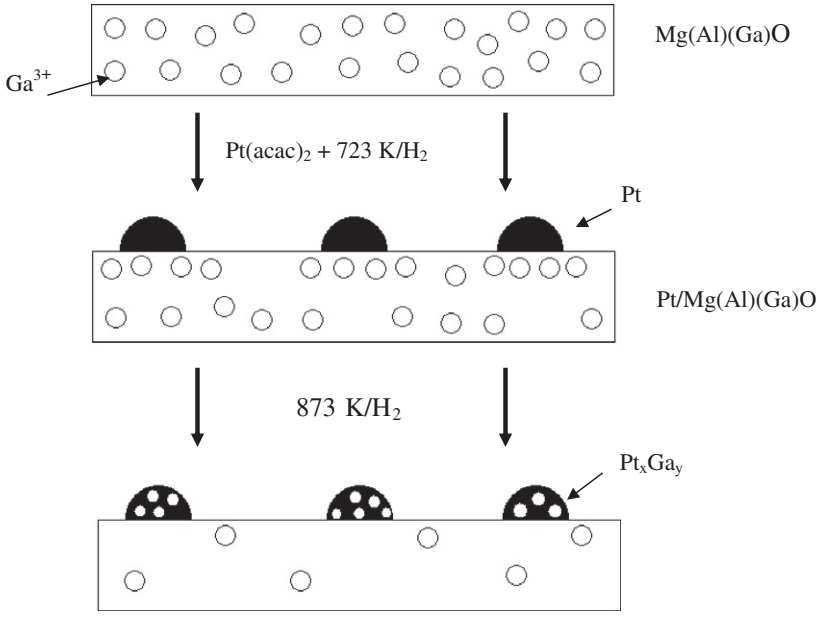

Fig. 13. Proposed mechanism for migration of Pt alloy formation during synthesis and reaction of Pt/Mg(Ga)(Al)O catalysts.

reduction at 873 K suggests that the individual metal particles of the Ga/Pt ratios vary from one to another.

The data acquired in this study suggest that upon reduction of Pt/Mg(Ga)(Al)O at temperatures above 773 K, a portion of the Ga^{3+} near the surface of the support is reduced to Ga atoms which then migrate and diffuse into the supported Pt nanoparticles, thereby forming PtGa alloys of varying composition. This interpretation is fully consistent with earlier studies of PtGa alloy formation on Pt/Ga_2O_3 and $Pt/Al_2O_3/Ga_2O_3$ [56,57]. TEM and STEM have also been used previously to infer the presence of PtGa alloys on Pt/Ga-ZSM-5, but the stoichiometry of the phases present was not determined [58]. In all cases, the presence of Pt is essential to enable the reduction of Ga^{3+}. Thus, it has been reported that Ga^{3+} in $GaCl_3/MgF_2$ could only be reduced at very high temperature, such as 1050 K [59]. However, the addition of Pt to this system lowered the temperature at which Ga^{3+} could be reduced to 713 K. A similar observation, that the reduction temperature of Ga^{3+} decreased by Pt presence, has been made for $PtGa/Al_2O_3$ [60], $Pt/Al_2O_3/Ga_2O_3$ [61], and Pt/H[Ga]ZSM-5 and Pt–Ga/H-ZSM-5 [61–69].

Therefore, we propose that during the reduction of Pt/Mg(Ga)(Al)O at elevated temperatures, H atoms formed on the surface of Pt particles spill over onto the support and initiate the reduction of Ga^{3+} cation to Ga atoms, which then interact with the supported Pt nanoparticles to GaPt alloys. Catalyst characterization by ICP, ^{71}Ga NMR, and Ga EXAFS suggest that only a small part of the total Ga in the support is consumed in this process and that most of the Ga^{3+} cations remain octahedrally coordinated in the support. The overall mechanism is proposed in Fig. 13.

4. Conclusion

A new method is reported for preparing PtGa bimetallic particles supported on a calcined, hydrotalcite-like support, Mg(Ga)(Al)O. Ga NMR spectra of the calcined support indicate that Ga^{3+} cations are present primarily in octahedral coordination. With increasing Ga/(Ga + Al) ratio, the support surface area decreases progressively and the size of the dispersed Pt particles increases, reflecting the need for Al atoms at the support surface in order to anchor the dispersed Pt. Information obtained from NMR, STEM-EDX, and Pt L_{III} edge EXAFS suggest that after reduction at 723 K, majority of the platinum is present in Pt and PtOx particles ranging in size from 1.4 to 2.2 nm. The size of the supported particles increased from an average of 1.2 nm to 2.2 nm as the Ga/(Ga + Al) ratio increased from 0 to 1. Upon H_2 reduction of Pt/Mg(Ga)(Al)O at 773–873 K, a portion of the Ga^{3+} cations near the surface are reduced to Ga atoms by H atoms spilled over from the supported Pt particles, leading to the formation of PtGa alloys ranging in Ga/Pt ratio from ~0.1 to 1.1.

Acknowledgments

This work was supported by Chevron Energy and Technology Company. The authors would like to thank Chris Canlas (Berkeley NMR facility) for his assistance in acquiring the Ga NMR spectra. TEM work was supported by ORNL's SHaRE User Facility, which is sponsored by the Scientific User Facilities Division, Office of Basic Energy Sciences, U.S. Department of Energy.

References

[1] O.A. Barias, A. Holmen, E.A. Blekkan, in: B. Delmon, G.F. Froment (Eds.), Catalyst Deactivation, Elsevier Science Publ. B.V., Amsterdam, 1994, pp. 519–524.
[2] A.A. Castro, Catalysis Letters 22 (1993) 123–133.
[3] S. de Miguel, A. Castro, O. Scelza, J.L.G. Fierro, J. Soria, Catalysis Letters 36 (1996) 201–206.
[4] J.M. Grau, E.L. Jablonski, C.L. Pieck, R.J. Verderone, J.M. Parera, Journal of Chemical Technology and Biotechnology 38 (1987) 105–113.
[5] M. Larsson, B. Andersson, O.A. Barias, A. Holmen, in: B. Delmon, G.F. Froment (Eds.), Catalyst Deactivation, Elsevier Science Publ. B.V., Amsterdam, 1994, pp. 233–240.
[6] L.C. Loc, N.A. Gaidai, S.L. Kiperman, H.S. Thoang, N.M. Podklenova, S.B. Kogan, Kinetika i Kataliz 32 (1991).
[7] H.H.C.M. Pinxt, B.F.M. Kuster, D.C. Koningsberger, G.B. Marin, Catalysis Today 39 (1998) 351–361.
[8] J.M. Ramallo-Lopez, G.F. Santori, L. Giovanetti, M.L. Casella, O.A. Ferretti, F.G. Requejo, The Journal of Physical Chemistry B 107 (2003) 11441–11451.
[9] G.J. Siri, J.M. Ramallo-López, M.L. Casella, J.L.G. Fierro, F.G. Requejo, O.A. Ferretti, Applied Catalysis A: General 278 (2005) 239–249.
[10] R.D. Cortright, J.A. Dumesic, Journal of Catalysis 148 (1994) 771–778.
[11] N. Nava, P. Del Angel, J. Salmones, E. Baggio-Saitovitch, P. Santiago, Applied Surface Science 253 (2007) 9215–9220.
[12] C. Vértes, E. Tálas, I. Czakó-Nagy, J. Ryczkowski, S. Göbölös, A. Vértes, J. Margitfalvi, Applied Catalysis 68 (1991) 149–159.
[13] E. Antolini, F. Colmati, E.R. Gonzalez, Journal of Power Sources 193 (2009) 555–561.
[14] L. Bednarova, C.E. Lyman, E. Rytter, A. Holmen, Journal of Catalysis 211 (2002) 335–346.
[15] V. Radmilovic, T.J. Richardson, S.J. Chen, P.N. Ross Jr., Journal of Catalysis 232 (2005) 199–209.
[16] A.T. Anghel, S.J. Jenkins, D.J. Wales, D.A. King, The Journal of Physical Chemistry B 110 (2006) 4147–4156.
[17] A.T. Anghel, D.J. Wales, S.J. Jenkins, D.A. King, The Journal of Chemical Physics 126 (2007) 044710–044713.
[18] C.R. Arumainayagam, G.R. Schoofs, M.C. McMaster, R.J. Madix, The Journal of Physical Chemistry 95 (2002) 1041–1047.
[19] S.M. Davis, G.A. Somojai, Hydrocarbon Conversion over Metal Surfaces, Elsevier Scientific, Amsterdam, 1982.
[20] Q. Ge, D.A. King, The Journal of Chemical Physics 110 (1999) 4699–4702.
[21] J.J.W. Harris, V. Fiorin, C.T. Campbell, D.A. King, The Journal of Physical Chemistry B 109 (2005) 4069–4075.
[22] M.C. McMaster, S.L.M. Schroeder, R.J. Madix, Surface Science 297 (1993) 253–271.
[23] D.J. Oakes, H.E. Newell, F.J.M. Rutten, M.R.S. McCoustra, M.A. Chesters, Chemical Physics Letters 253 (1996) 123–128.
[24] G. Papoian, J.K. Norskov, R. Hoffmann, Journal of the American Chemical Society 122 (2000) 4129–4144.
[25] P.K. Wang, C.P. Slichter, J.H. Sinfelt, The Journal of Physical Chemistry 89 (1985) 3606–3609.
[26] P.-K. Wang, J.-P. Ansermet, S.L. Rudaz, Z. Wang, S. Shore, C.P. Slichter, J.H. Sinfelt, Science 234 (1986) 35–41.
[27] G.W. Watson, R.P.K. Wells, D.J. Willock, G.J. Hutchings, The Journal of Physical Chemistry B 104 (2000) 6439–6446.
[28] J.F. Weaver, M.A. Krzyzowski, R.J. Madix, The Journal of Chemical Physics 112 (2000) 396–407.
[29] S.M.K. Airaksinen, M.A. Bañares, A.O.I. Krause, Journal of Catalysis 230 (2005) 507–513.
[30] A.V. Zeigarnik, R.E. Valdes-Perez, O.N. Myatkovskaya, The Journal of Physical Chemistry B 104 (2000) 10578–10587.
[31] S.A. Bocanegra, A.A. Castro, O.A. Scelza, S.R. de Miguel, Applied Catalysis A: General 333 (2007) 49–56.
[32] S.A. Bocanegra, A. Guerrero-Ruiz, S.R. de Miguel, O.A. Scelza, Applied Catalysis A: General 277 (2004) 11–22.
[33] R.D. Cortright, J.M. Hill, J.A. Dumesic, Catalysis Today 55 (2000) 213–223.
[34] M. Tasbihi, F. Feyzi, M.A. Amlashi, A.Z. Abdullah, A.R. Mohamed, Fuel Processing Technology 88 (2007) 883–889.
[35] Y. Zhang, Y. Zhou, A. Qiu, Y. Wang, Y. Xu, P. Wu, Catalysis Communications 7 (2006) 860–866.
[36] T. Waku, J.A. Biscardi, E. Iglesia, Journal of Catalysis 222 (2004) 481–492.
[37] D. Akporiaye, S.F. Jensen, U. Olsbye, F. Rohr, E. Rytter, M. Ronnekleiv, A.I. Spjelkavik, Industrial & Engineering Chemistry Research 40 (2001) 4741–4748.
[38] A. Virnovskaia, S. Jørgensen, J. Hafizovic, Ø. Prytz, E. Kleimenov, M. Hävecker, H. Bluhm, A. Knop-Gericke, R. Schlögl, U. Olsbye, Surface Science 601 (2007) 30–43.
[39] V. Galvita, G. Siddiqi, P. Sun, A.T. Bell, Journal of Catalysis 271 (2010) 209–219.
[40] G. Siddiqi, P. Sun, V. Galvita, A.T. Bell, Journal of Catalysis 274 (2010) 200–206.
[41] M. Newville, J. Synchrot. Radiat. 8 (2001) 322–324.
[42] B. Ravel, M. Newville, J. Synchrot. Radiat. 12 (2005) 537–541.
[43] G.V. Raynor, A Handbook of Lattice Spacings and Structures of Metals and Alloys, Pergamon Press, 1958.
[44] P. Villars, L.D. Calvert, W.B. Pearson, Pearson's Handbook of Crystallographic Data for Intermetallic Phases, ASM International, Materials Park, OH, 1991.
[45] M. Bellotto, B. Rebours, O. Clause, J. Lynch, D. Bazin, E. Elkaim, The Journal of Physical Chemistry 100 (1996) 8527–8534.
[46] R. Bastiani, I.V. Zonno, I.A.V. Santos, C.A. Henriques, J.L.F. Monteiro, Brazilian Journal of Chemical Engineering 21 (2004) 193–202.
[47] S. Kannan, D. Kishore, K. Hadjiivanov, H. Knozinger, Langmuir 19 (2003) 5742–5747.
[48] H.S. Panda, R. Srivastava, D. Bahadur, Materials Research Bulletin 43 (2008) 1448–1455.

[49] F.M. Labajos, V. Rives, M.A. Ulibarri, Journal of Materials Science 27 (1992) 1546–1552.
[50] J. Shen, M. Tu, C. Hu, Journal of Solid State Chemistry 137 (1998) 295–301.
[51] S.M. Bradley, R.F. Howe, R.A. Kydd, Magnetic Resonance in Chemistry 31 (1993) 883–886.
[52] D. Massiot, R. Revel, C. Magnenet, D. Bazin, Solid State Nuclear Magnetic Resonance 16 (2000) 103–108.
[53] D. Massiot, T. Vosegaard, N. Magneron, D. Trumeau, V. Montouillout, P. Berthet, T. Loiseau, B. Bujoli, Solid State Nuclear Magnetic Resonance 15 (1999) 159–169.
[54] J.H. Kwak, J. Hu, D. Mei, C.-W. Yi, D.H. Kim, C.H.F. Peden, L.F. Allard, J. Szanyi, Science 325 (2009) 1670–1673.
[55] S. Abelló, J. Pérez-Ramírez, Microporous and Mesoporous Materials 96 (2006) 102–108.
[56] F. Domínguez, J. Sánchez, G. Arteaga, E. Choren, Journal of Molecular Catalysis A: Chemical 228 (2005) 319–324.
[57] N. Iwasa, T. Mayanagi, N. Ogawa, K. Sakata, N. Takezawa, Catalysis Letters 54 (1998) 119–123.
[58] P. Mériaudeau, G. Sapaly, C. Naccache, Journal of Molecular Catalysis 81 (1993) 293–300.
[59] Y.C. Cao, X.Z. Jiang, Journal of Molecular Catalysis A: Chemical 242 (2005) 119–128.
[60] E.L. Jablonski, A.A. Castro, O.A. Scelza, S.R. de Miguel, Applied Catalysis A: General 183 (1999) 189–198.
[61] F. Domínguez, G. Carruyo, R. Andrade, R. Solano, D. Rodríguez, J. Sánchez, G. Arteaga, Catalysis Letters 123 (2008) 207–212.
[62] M. Mediavilla, L. Melo, Y. Díaz, J.L. Brito, A. Albornoz, R. Solano, Microporous and Mesoporous Materials 102 (2007) 86–94.
[63] L. Melo, Y. Díaz, M. Mediavilla, A. Albornoz, J.L. Brito, Catalysis Letters 97 (2004) 105–109.
[64] Y. Diaz, L. Melo, M. Mediavilla, A. Albornoz, J.L. Brito, Journal of Molecular Catalysis A: Chemical 227 (2005) 7–15.
[65] L. Melo, A. Llanos, M. Mediavilla, D. Moronta, Journal of Molecular Catalysis A: Chemical 177 (2002) 281–287.
[66] E.S. Shpiro, D.P. Shevchenko, E.V. Dmitriev, O.P. Tkachenko, K.M. Minachev, Applied Catalysis A: General 107 (1994) 165–180.
[67] B. Zheng, W. Hua, Y. Yue, Z. Gao, Journal of Catalysis 232 (2005) 143–151.
[68] S.E. Collins, M.A. Baltanás, J.L. Garcia Fierro, A.L. Bonivardi, Journal of Catalysis 211 (2002) 252–264.
[69] V.V. Rozanov, O.V. Krylov, Uspekhi Khimii 66 (1997) 117–130.